Metrol. Meas. Syst., Vol. 26 (2019) No. 3, pp. 517–530
DOI: 10.24425/mms.2019.129576

METROLOGY AND MEASUREMENT SYSTEMS
Index 330930, ISSN 0860-8229
www.metrology.pg.gda.pl

DEVELOPMENT OF AN ACOUSTO-OPTIC SYSTEM FOR HYPERSPECTRAL IMAGE SEGMENTATION

César Isaza[1)], Julio M. Mosquera[2)], Gustavo A. Gómez-Méndez[2)], Jonny P. Zavala-De Paz[1)], Ely Karina-Anaya[1)], José A. Rizzo-Sierra[1)], Omar Palillero-Sandoval[3)]

1) *Universidad Politécnica de Querétaro, Carretera Estatal 420 S/N, C.P. 76240, El Marqués, Querétaro, México* (*cesar.isaza@upq.mx*, ✉*jonny.zavala@upq.edu.mx*, +01 442 101 9000, *karina.anaya@upq.mx*, *jose.rizzo@upq.mx*)
2) *Universidad del Quindío, Facultad de Física, Armenia, Colombia* (*jcmosquera@uniquindio.edu.co*, *tavo1094@hotmail.com*)
3) *Universidad Autónoma del Estado de Morelos, Center for Research in Engineering and Applied Science, México* (*omar.palillero.@uaem.mx*)

Abstract

Image segmentation is a typical operation in many image analysis and computer vision applications. However, hyperspectral image segmentation is a field which have not been fully investigated. In this study an analogue-digital image segmentation technique is presented. The system uses an acousto-optic tuneable filter, and a CCD camera to capture hyperspectral images that are stored in a digital grey scale format. The data set was built considering several objects with remarkable differences in the reflectance and brightness components. In addition, the work presents a semi-supervised segmentation technique to deal with the complex problem of hyperspectral image segmentation, with its corresponding quantitative and qualitative evaluation. Particularly, the developed acousto-optic system is capable to acquire 120 frames through the whole visible light spectrum. Moreover, the analysis of the spectral images of a given object enables its segmentation using a simple subtraction operation. Experimental results showed that it is possible to segment any region of interest with a good performance rate by using the proposed analogue-digital segmentation technique.

Keywords: hyperspectral imaging, acousto-optic system, image segmentation.

1. Introduction

The development of imaging processing techniques has reached limits which until recently were considered insurmountable. In particular, the development of specialized algorithms accompanied by high-resolution sensors have reduced the computation time of some image processing techniques, near what is typically called real time [1]. In addition, it is well known that most of image processing techniques demand a pre-processing step to extract a region of interest.

(*i.e.*, techniques such as, inter alia: object detection, tracking). Moreover, the generalization of algorithms in image processing and computer vision, presents a difficult problem that a few times is solved with good results [2]. Because of the complexity of this operation, many methods are specifically adjusted to solve restricted problems. Furthermore, small changes in lighting conditions or in the environment in general, lead to losing efficiency of algorithms, the effect that could be overcome by using more complex methods or hardware [3, 4].

Due to the above, the segmentation of a region of interest is a specific process for each application that requires variation in most of the algorithms. Therefore, the computational cost is undesirable and sometimes real-time processing becomes complex. Moreover, the quality of the segmentation is directly proportional to the complexity of the developed algorithm, which again leads to a higher computational cost [5].

A proposed improvement has emerged while one combines digital and analogue segmentation techniques, especially techniques based on the use of spectral images to reduce the processing time of images, ensuring a good segmentation quality [6, 7]. Among these techniques, there has been an interesting idea consisting in the use of *acousto-optic tuneable filters* (AOTFs), considered to be one of the best answers for implementing analogue-digital systems [8, 9]. This is due to the fundamental simplicity and intrinsic speed of optical spectrum analysers [11]. However, the judgment on whether these methods are better has remained in qualitative considerations, given that there are no comparative studies to quantitatively determine the goodness of using AOFs against all different existing digital techniques [9]. Thus, it is necessary to calculate the segmentation quality and quantitatively assess the results achieved through processing data obtained from hyperspectral images acquired by AOTFs. In this work, a comparative study using hyperspectral images captured by means of AOTFs is presented. In addition, the work presents the quantitative assessment of benefits of using AOTFs. That is, a digital-analogue image segmentation method and a quantitative evaluation of its efficiency is proposed.

2. Spectral and hyperspectral image segmentation

In spectroscopy and photography, the spectral image term is used to describe matrix information that is collected at every location within some particular spectral range. Typically, three spectral bands are used: red, green, and blue.

Many spectral image segmentation techniques are available in the literature. Some of them transform a colour image into a grey level one. In [17] there is presented a review of some works that use Markov Random Field models, Neural Network architectures, fuzzy and non-fuzzy techniques applied to colour and grey level images. In 2001, Zhang [18] presented a review of methods used to analyse and compare several evaluation techniques to classify the performance of different metrics. In this study there is relevant the task of quantitative evaluation of the segmentation procedure. Considering colour images, in [3] there is presented a survey of several segmentation techniques. Basically, the authors report approaches to segmenting monochrome images. The main techniques used there are, inter alia: histogram thresholding, characteristic feature clustering, edge detection, region-based methods, fuzzy techniques, neural networks.

With the growing research on image segmentation, several image segmentation techniques were developed for optical remote sensing. In [23] there is presented a review of selected papers from image processing journals, conferences, books, dissertations, and theses. The authors categorized all techniques into the following classes: image-driven approach, model-driven ap-

Metrol. Meas. Syst., Vol. 26 (2019), No. 3, pp. 517–530
DOI: 10.24425/mms.2019.129576

proach (object background model, Markov random field model, fuzzy model, neural model, multi-resolution model, and watershed model); based on the measure of homogeneity (spectral and textural features, shape and size features, context, temporal, and prior knowledge).

Recently, Devarshi and Pinal [24] presented a review of image segmentation clustering algorithms. Their strategy attempts to discover a set of consequential groups from pixel information of an image. In particular, the cluster algorithms considered to segment images were: K-means, fuzzy c-means, expectation maximization, hierarchical, and self-organizing maps.

Hyperspectral and multispectral imaging is another special area of physics that collects and processes information from the electromagnetic spectrum [19–22]. However, the main difference between hyperspectral and multispectral imagery is the number of bands and their widths. In particular, multispectral images consider only a few spectral bands with a significant difference between them. In contrast, hyperspectral images are collected continuously through the visible and near-infrared electromagnetic spectrum. In other words, the hyperspectral acquisition is a continuous process, while the multispectral – a discrete one. Following the above, the hyperspectral image segmentation has been applied in such fields as medicine, quality inspection of postharvest products, and remote sensing. In 2007, Guillame [10] presented a methodology for the morphological segmentation of hyperspectral images. This approach used the watershed transform to obtain markers and vectorial gradient information from the image. Similarly, in [12] the authors deal with the problem of hyperspectral image segmentation using data to integrate the spatial and spectral information. A different approach is presented in [13], where a semi-supervised segmentation algorithm is introduced to deal with high-dimensional data that represent hyperspectral images. In the field of medicine, some methods to segment hyperspectral images have been proposed. In [14] there is presented a tongue segmentation method in hyperspectral images. In this work, the authors use support vector machines to combine spatial and spectral information to provide a tongue segmentation. In tomography diagnosis [15] there are used segmented hyperspectral images of bioluminescence optical tomography. In [16] there is provided an introduction to hyperspectral images, considering the equipment and methods of image acquisition and processing. In particular, the authors describe the use of hyperspectral images to food safety and quality assessment that may include contaminant detection, defect identification, constituent analysis and quality evaluation. Similarly, in [25] there is presented a review of works that use hyperspectral imaging in the inspection of fruit and vegetables. The authors describe different technologies available to acquire spectral images and their use in non-destructive inspection of the internal and external features of food products.

3. Material and methods

3.1. Acousto-optic tuneable filter

The spectral images were acquired using an acousto-optic cell. A birefringent crystal having a piezoelectric transducer attached to one end that is excited with a radio-frequency signal, constitutes the AO cell. The piezoelectric transducer generates ultrasonic waves travelling through the crystal. Thus, the crystal behaves as a diffraction grating because the compression expansion zones induce variation of a refractive index (Fig. 1) [8]. The refractive index n is modulated by the acoustic wave travelling in the crystal, with a spatial period equal to the wavelength of sound, given by:

$$\Lambda = \frac{V}{f}, \tag{1}$$

where Λ is a wavelength of the sound wave; V – a phase velocity of the sound wave in the crystal; f – the sound wave frequency. Therefore, in the crystal the ultrasonic wave generates a spatial diffraction grating. In this case, if a non-polarized light beam (an image carrier) is incident on the cell, as a result of the acousto-optic interaction, one obtains two diffracted rays that emerge $at + 1$, 1 diffraction order. Fig. 1 shows a zero-order ray corresponding to the non-diffracted beam, and the +1 diffraction order ray is spatially shifted in the same direction of the acoustic wave movement. The 1-order ray is shifted to the opposite side of the non-diffracted beam [26].

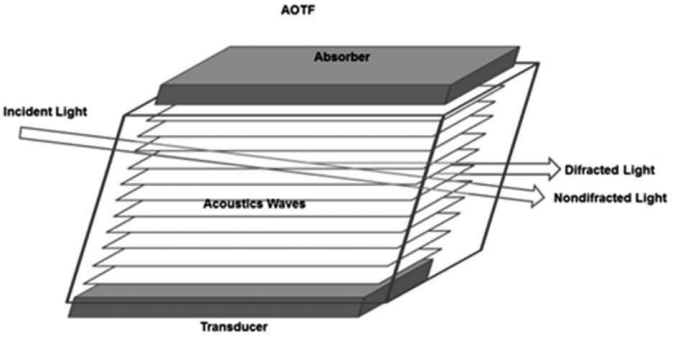

Fig. 1. Acousto-optic tuneable filter.

As is well known, any periodic structure has the property of spectrally decomposing light. As mentioned, the cell behaves as a spatial diffraction grating and AO interaction in the crystal occurs under strict compliance with Bragg's law [27, 28]:

$$\sin\theta = \frac{\lambda f}{2nv}, \tag{2}$$

where θ is a light incidence angle on the crystals and λ – a wavelength of light diffracted. The AOTF extracts a narrow band of wavelengths around λ from the entire spectrum of the incident light. From relation (2) it follows that the colour of the diffracted light is a function of the RF signal frequency; therefore, setting a certain frequency f, a spectral component λ corresponding to (f) is obtained. Since the frequency f can be electronically controlled at times of order 10^{-4} s, AOTF enables to acquire spectral images of a scene one wants to capture. Note that each object in the scene has its own spectral components, and therefore it is expected that different spectral components (different frames) of the scene will contain different objects (Fig. 2).

3.2. Acousto-optic system

Depending on the AO interaction geometry and material used, each AO cell has a specific operating bandwidth of coverage. The AO cell used here may acquire images in a wide bandwidth that are within the visible light range (380 nm −720 nm), however in this work the images were acquired from between 470 nm and 645 nm.

The acousto-optic system for acquisition of spectral images (Fig. 2) consists of a CCD Hitachi camera, an optical zoom Tokina brand, and – between the camera and the zoom – an *acousto-optic tuneable filter* (FAO), *i.e.* the AO cell made of Parateluria (TeO2) crystal [28]. An RF generator is needed in order to obtain the RF excitation signal to produce the acoustic wave on the AO filter. A PCI high-speed video grabber EPIX digitizes the spectral images captured by the AO system.

Metrol. Meas. Syst., Vol. 26 (2019), No. 3, pp. 517–530
DOI: 10.24425/mms.2019.129576

3.3. Data set

An algorithm developed in V++®controls the acousto-optic system. The code simultaneously controls the camera and the *radio frequency* (RF) generator, which acts as a bridge between the software and the AOTF, to acquire a package of hyperspectral images in grey level (Fig. 2).

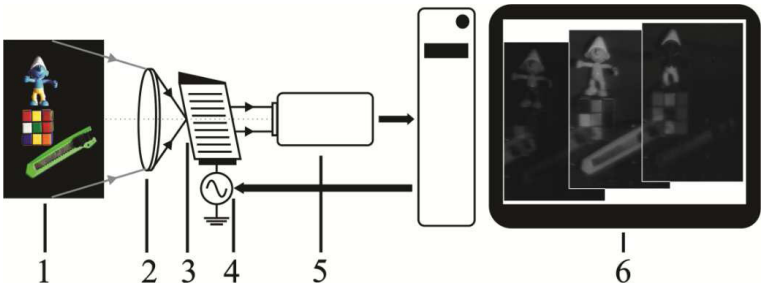

Fig. 2. 1) scene; 2) lens; 3) acousto-optical tuneable filter; 4) RF generator; 5) CCD camera; 6) computer.

The acquisition can be done in RGB format, but this process is only informative, since each image is actually highly monochromatic, that is, it corresponds to a single wavelength of incident light (Fig. 3).

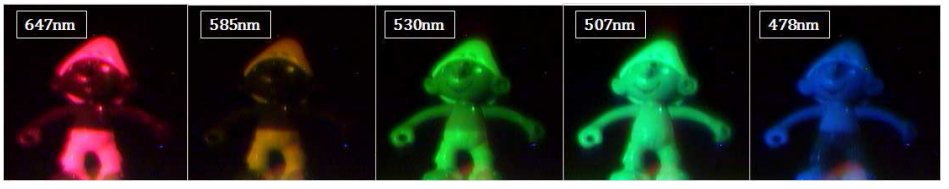

Fig. 3. A sample of hyperspectral images in RGB format.

The control code is initialized from a value of 85000 that at the RF generator corresponds to $f = 85$ MHz output. This excitation signal corresponds to a wavelength of $\lambda = 645$ m for the diffracted light. The sweep of the entire spectral range is performed in steps of 2 nm. In each step, the camera automatically captured one frame which was stored on a hard disc. This process stops when the shortest wavelength of $\lambda = 453$ nm is reached. Thus, a total of 96 hyperspectral images corresponding to the visible spectrum are captured. It is important to notice that this system has no moving parts and has a fully electronic control. Fig. 4 illustrates some hyperspectral images.

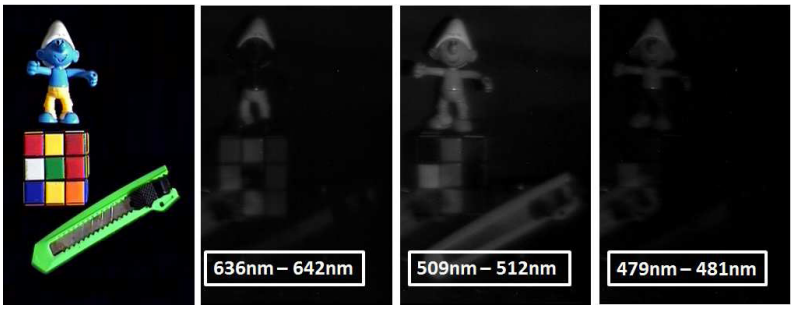

Fig. 4. Samples from the hyperspectral image data set.

4. Segmentation process

Segmentation processes may attempt to find out the boundaries of an object and then locate the object itself as the region of interest in the image. Moreover, to acquire spectral frames from a scene, usually a pre-segmented image is obtained and if objects in the scene are not overlapping, the segmentation can be performed through simple subtraction operations. In the case of overlapping, it is necessary to complement this task using morphological operations to define a mask that represents the object to be segmented. Based on the above, the segmentation process in this research was carried out considering two different strategies. The first one assumes the user manually analysing all hyperspectral images and recognizing particular features in the regions of interest to be segmented. The second one uses a semi-automatic segmentation learning technique where the user manually selects a region of interest and the algorithm automatically chooses the optimal pair of images at different wavelengths, where the segmentation procedure generates the optimal result.

4.1. Manual segmentation technique

In this section the method of manual segmentation of the image is presented. Thus, in this stage, the user should consider all hyperspectral images and split the visual information into two regions of interest. The first region holds the information of the object of interest to be segmented, while the other – of the rest of the image. This step gives to the user information about the changes in intensity of both regions. Then, the user should choose a pair of images where the region of interest of the object changes drastically, and the region of non-interest does not change too much. If the above criteria are used and a simple subtraction operation is applied to the images, an output image will be obtained with large values for the region of interest of the object, while with lower ones for the region of non-interest. An example of this procedure is presented in Fig. 5. Thus, two hyperspectral images are presented. One of them represents the scene captured at 498.34 nm (Fig. 5a), while the other – at 631.11 nm (Fig. 5b). Fig. 5c, illustrates the result of their subtraction. In the example, the region of interest considered contains the pixels belonging to a Smurf toy.

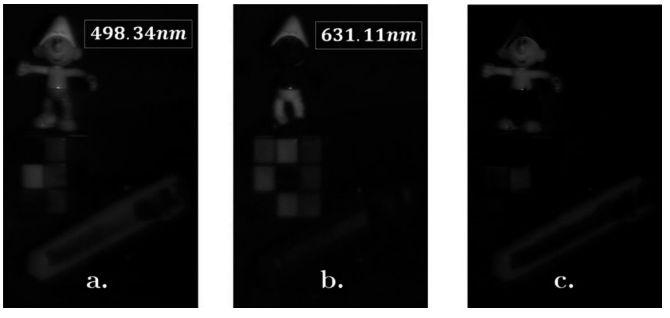

Fig. 5. An example of the manual segmentation method. The output image (c) is obtained by subtraction of images (a) and (b).

4.2. Semi-automatic segmentation technique

Semi-automatic image segmentation techniques combine the information that the user generates manually and the information gathered from automatic image analysis algorithms. Both kinds of data are used in order to segment a region of interest of an object. Additionally, in this

Metrol. Meas. Syst., Vol. 26 (2019), No. 3, pp. 517–530
DOI: 10.24425/mms.2019.129576

study all segmentation operations were performed in MATLAB 2013B® using the hyperspectral data set of images acquired with the AO system. In particular, the proposed method consists of the following stages:

1. The user selects manually the region of interests in a scene. These regions are going to be considered as a mask, and the ground truth to quantitatively and qualitatively evaluate the segmentation results (see Fig. 6).

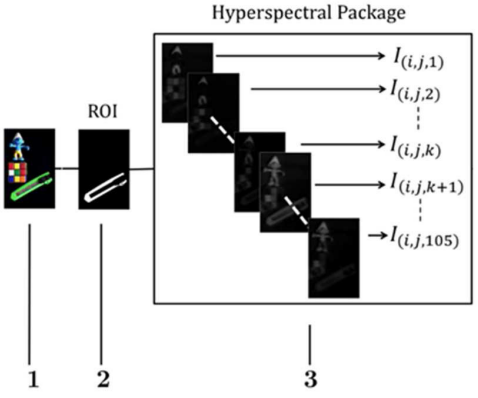

Fig. 6. Semi-automatic method: 1 – scene; 2 – region of interest; 3 – hyper-spectral package.

2. A hyperspectral sequence of 96 images of the scene is obtained from wavelengths of 470 to 645 nm.
3. The subtraction operations for permutations of pairs of masked images corresponding to different wavelengths are computed over the full spectrum (see Fig. 7).

$$\forall\, I_{(i,j,k)} \neq 0;$$

$$R_{<x>} = \sum_{k=1}^{n-1} \sum_{m=k+1}^{n} \sum_{i=1}^{i_{max}} \sum_{j=1}^{j_{max}} \frac{\left| I_{(i,j,k)} - I_{(i,j,m)} \right|}{p * i * j},$$

$$n = Number\ of\ Hyperspectral\ Images$$

$$k = Number\ of\ Substraction\ Operations$$

$$p = Pixel\ Bit\ Resolution\ -\ 255\ (8\ bits)$$

$$\forall\, x = 1,\ 2,\ \ldots\ \tau$$

$$Where\ \tau = \frac{(n-1)^2 + (n+1)}{2}$$

Fig. 7. Subtraction and normalization operations.

4. A normalization procedure is applied to all subtracted images. This step takes into account the resolution of the image (rows and columns), and the highest different pixel value

estimated by the subtraction operation. In particular, this step avoids to measure intensity values that vary in terms of size of the region that was analysed. After this step, all values are normalized into values between zero and one.

5. From all subtracted images the total amount of reflectance is measured and allocated into a one-dimensional vector. This output subtraction vector is used to automatically look for the highest point, which represents the total amount of reflectance obtained from a pair of images at different wavelengths. Furthermore, this value corresponds to the pair of images that represent the maximum change in the spectral information of the region of interest to be segmented (see Fig. 8).

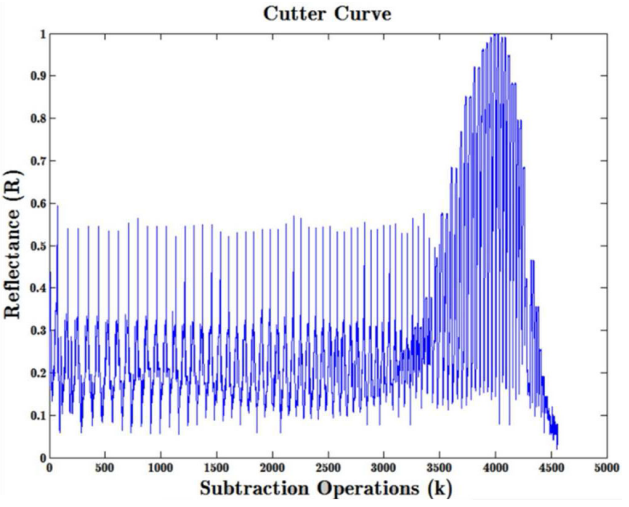

Fig. 8. Reflectance curve.

In general, the previous steps describe a training stage that may be used in automatic object detection from hyperspectral images. Figs. 6, 7 and 8 illustrate the semi-automatic method to segment a region of interest from hyperspectral images.

5. Experimental results

In this section, the results of the procedure of segmenting a region of interest from hyperspectral images are presented. The evaluation is considered to be not only the quantitative but also the qualitative one. By using the current proposal, several experiments that include a scene with three objects were performed.

5.1. Qualitative evaluation

The qualitative evaluation was performed considering three objects that appear in the scene of study (see Fig. 4). Fig. 9 shows the reflectance curves of the subtracted and normalized images, and the optimal hyperspectral images that represent the highest reflectance difference for the region of interest. Then, Fig. 10 illustrates the ground truth and the results of the segmentation process obtained with the manual and semiautomatic methods.

Metrol. Meas. Syst., Vol. 26 (2019), No. 3, pp. 517–530
DOI: 10.24425/mms.2019.129576

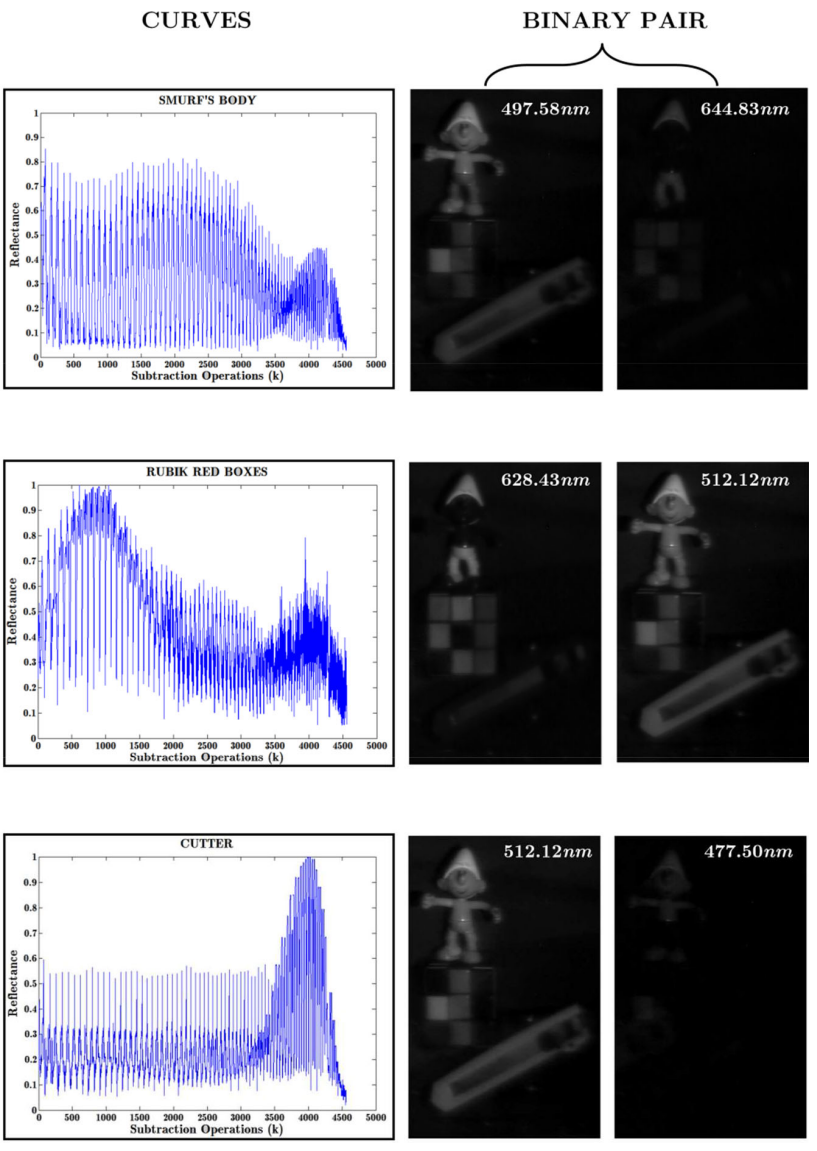

Fig. 9. Pairs of optimal hyperspectral images obtained by using the semi-automatic method to segment an object.

Analysing the first row of Fig. 10 (Smurf toy), it is possible to notice that both manual and semi-automatic strategies give similar visual results. However, for the second object (Rubik cube) there are important differences between the compared methods. Here, the most important aspect to notice is that areas outside the region of interest are appearing with greater intensity in the manual segmentation than in the semiautomatic one. Nonetheless, the results for the third object (cutter) obtained with the manual method are better than with the semi-automatic one. This fact can be visualized in the intensity of pixels that belong to the body of the Smurf.

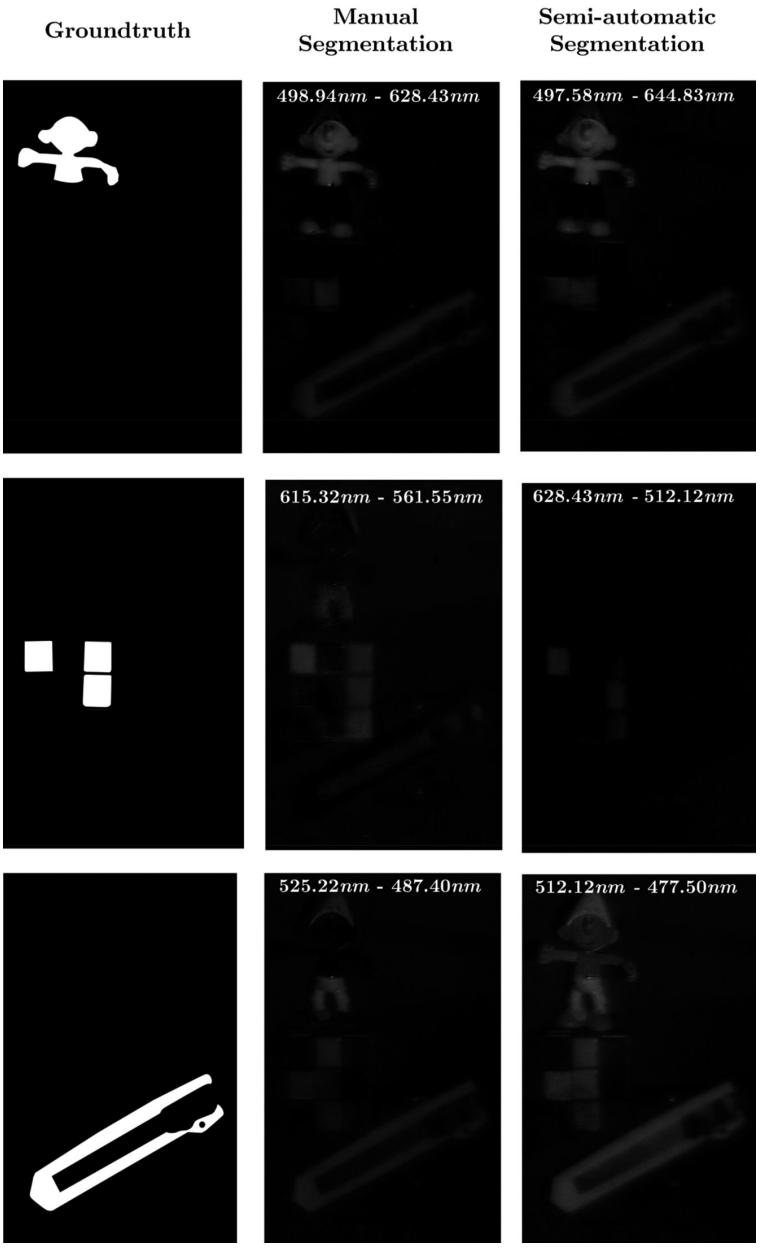

Fig. 10. Qualitative evaluation with manual and semi-automatic methods of segmenting hyperspectral images.

5.2. Quantitative evaluation

The quantitative evaluation considers an average image that represents the main spectral information of the full spectrum analysed. Since the hyperspectral information varies for each object, it is not possible to select a single wavelength as the reference image to extract the ground

Metrol. Meas. Syst., Vol. 26 (2019), No. 3, pp. 517–530
DOI: 10.24425/mms.2019.129576

truth. Thus, the quantitative evaluation was performed using *receiver operating characteristic* (ROC) parameters of the regions of interest that belong to the object of study, and of the background of the scene. Fig. 11 shows the ROC curves obtained for manual and Fig. 12 – for semi-automatic segmentation techniques. The ROC parameters considered in this study are:

– *True Positive* (TP): pixels that appear in the ground truth (white), and in the segmented image computed with the manual (see Fig. 12) or semi-automatic (see Fig. 13) method as part of the object of interest (white).
– *True Negative* (TN): pixels that appear in the background (black), and in the segmented image as part of the area outside the region of interest (black).

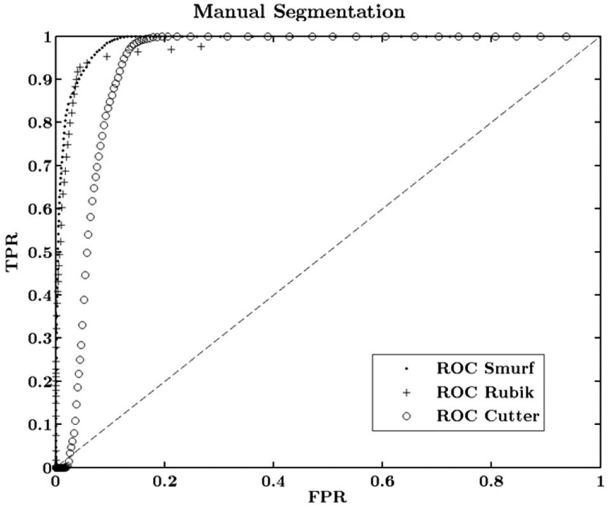

Fig. 11. A *receiver operating characteristic* (ROC) curve for the manual segmentation technique.

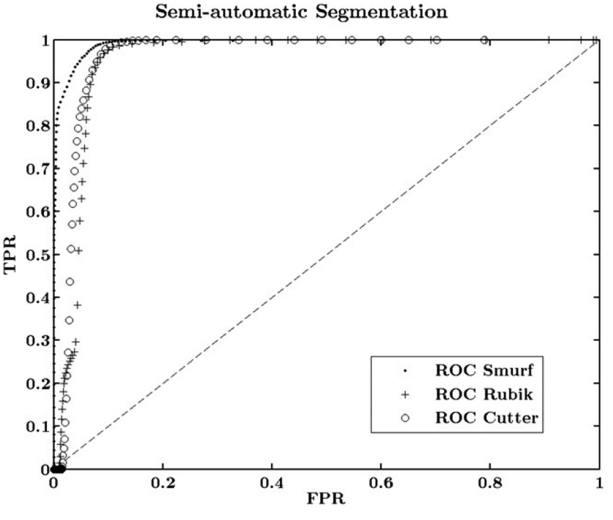

Fig. 12. A *receiver operating characteristic* (ROC) curve for the semi-automatic segmentation technique.

– *False Positive* (FP): pixels that appear in the background (black), and in the segmented image as part of the object of interest (white).
– *False Negative* (FN): pixels that appear in the ground truth (white), and in the segmented image as part of the area outside the region of interest (black). The ROC curve is obtained by considering a threshold value applied to the segmented image. Then, the *false positive rate* (FPR), and *true positive rate* (TPR) are computed using FPR = FP/(FP + TN), and TPR = TP/(TP + FN).

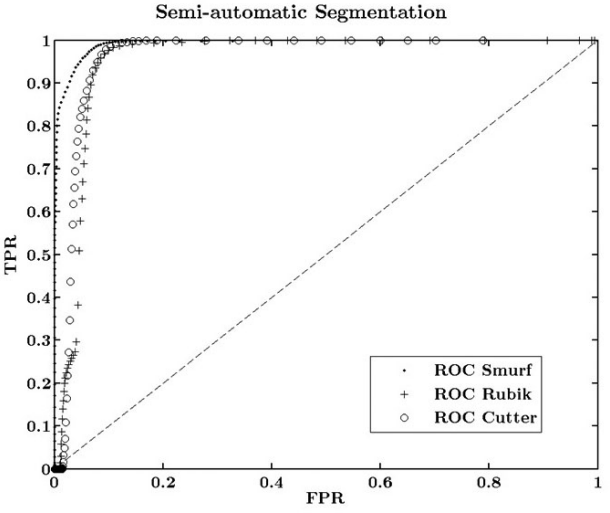

Fig. 13. A receiver operating characteristic (ROC) curve for the semi-automatic segmentation technique.

The ROC curves express the relative error of the segmentation process changing the threshold values. Since the *optimal threshold* (Th) is the nearest point of the curve to the upper left corner, a magnitude vector parameter ($\mathbf{V}\perp$) is computed in order to compare the segmentation procedures of all objects of interest. Moreover, all curves show that both manual and semi-automatic segmentation techniques have an efficiency above 90% (see TPR values of the nearest point of the curve to the upper-left corner).

Table 1 presents the quantitative evaluation results of the manual and semi-automatic segmentation techniques.

Table 1. Data ROC.

Object	Image	$\|\mathbf{V}\perp\|$	Th	TP	TN	FP	FN	TPR	FPR
Smurf	Ground truth	−0.06	−26	12576	348384	0	0	1	0
	Semi-automatic	0.08	34	12046	330232	18152	530	0.95	0.05
	Manual			11943	325293	23091	633	0.94	0.06
Rubik	Ground truth	−0.09	−21	10172	350788	0	0	1	0
	Semi-automatic	0.08	6	9745	320760	30028	427	0.95	0.08
	Manual			9445	335039	15749	727	0.92	0.04
Cutter	Ground truth	−0.09	−21	22257	338703	0	0	1	0
	Semi-automatic	0.13	34	21504	309426	29277	753	0.96	0.08
	Manual			21098	296165	42538	1159	0.94	0.12

Metrol. Meas. Syst., Vol. 26 (2019), No. 3, pp. 517–530
DOI: 10.24425/mms.2019.129576

Using the values obtained from the ROC curves it is possible to compare the two segmentation strategies. In particular, the TPR column contains the following information:

- Smurf: The semi-automatic segmentation method has an efficiency of 94%, while the manual −95%.
- Rubik: The semi-automatic method has an efficiency of only 92%, while the manual −95%.
- Cutter: The semi-automatic method has an efficiency of 94%, while the manual −96%.

6. Conclusions

An important element in the field of image analysis is the segmentation process that may contribute to understanding the scene of study. In particular, the segmentation of hyperspectral images is a research topic that demands a lot of effort not only in the design and implementation of the acquisition systems, but also in the methods used to extract the regions of interest. In this context, a new semi-automatic hyperspectral image segmentation technique is proposed using acousto-optic tuneable filters as the acquisition system. The results show that hyperspectral images can be segmented by using a subtraction strategy, where only a pair of images acquired in a particular wavelength are required. Moreover, a qualitative and quantitative evaluation of the segmentation methods used in this work were performed. Considering the above, it is possible to conclude that the semi-automatic segmentation strategy is better than the manual method. Quantitatively, the *true positive rate* (TPR) is around 95%, while the *false positive rate* (FPR) is less than 0.1%. Nevertheless, the proposed methodology significantly improves the process of hyperspectral image segmentation and opens a new field in computer vision to understand complex images acquired with hyperspectral systems.

The future work will focus on the use of the reflectance curve obtained from the full spectrum to characterize any object that appears in a complex scene that may be located either indoors or outdoors. This feature extraction process will contribute to the development of new methods to detect and track any object from a sequence of images (video).

References

[1] Lee, J., Shinozuka, M. (2006). Real-time displacement measurement of a flexible bridge using digital image processing techniques. *Experimental Mechanics*, 46(1), 105–114.

[2] Meer, P., Mintz, D., Rosenfeld, A., Yoon, D. (1991). Robust regression methods for computer vision: A review. *International Journal of Computer Vision*, 6(1), 59–70.

[3] Cheng, H., Jiang, X, Sun Y., Wang, J. (2001). Color image segmentation: advances and prospects. *Pattern recognition*, 34(12), 2259–2281.

[4] Burnett, C., Blaschke, T. (2003). A multi-scale segmentation/object relationship modelling methodology for landscape analysis. *Ecological Modelling*, 168(3), 233249.

[5] Tang, L., Tian, L., Steward, F. (2000). Color image segmentation with genetic algorithm for in-field weed sensing. *Transactions of the ASAE*, 43(4), 1019–1027.

[6] Ryherd, S., Woodcock, C. (1996). Combining spectral and texture data in the segmentation of remotely sensed images. *Photogrammetric engineering and remote sensing*, 62(2), 181–194.

[7] Mosquera, J., Isaza, C., Gómez, G. (2012). Technical analog-digital for segmentation of spectral images acquired with an acousto-optic system. *XVII Symposium of Image, Signal Processing and Artificial Vision (STSIVA)*.

[8] Voloshinov, V., Molchanov, V., Mosquera, J. (1996). Spectral and polarization analysis of optical images by means of acousto-optics. *Optics & Laser Technology*, 28(2), 119–127.

[9] Narasimha, S., Feng, J., Emir, Y., Susan, K., Sudhir, B., Jolanta, S. (2018). Acousto-optic tunable filter based spectrapolarimeter for extraction of Stokes and Mueller matrices. *Proc. SPIE 10655, Polarization: Measurement, Analysis, and Remote Sensing XIII*.

[10] Guillaume, N., Angulo, J., Dominique, J. (2007). Morphological segmentation of hyperspectral images. *Image. Anal. Stereol*., 26,101–109.

[11] Turpin, T. (1981). Spectrum analysis using optical processing. *Proc. of the IEEE*, 69(1), 79–92.

[12] Antonio, P., Atli, J., Boardman, J., Brazile, J., Bruzzone, L., Camps, G., Chanussot, J., Fauvel, M., Gamba, P. (2009). Recent advances in techniques for hyperspectral image processing. *Remote sensing of environment*, 113(1), S110–S122.

[13] Li, J., Bioucas, J., Plaza, A. (2010). Semisupervised hyperspectral image segmentation using multinomial logistic regression with active learning. *IEEE Transactions on Geoscience and Remote Sensing*, 48(11), 4085–4098.

[14] Liu, Z., Yan, J., Zhang, D., Li, Q. (2007). Automated tongue segmentation in hyperspectral images for medicine. *Journal of Applied optics*, 46(34), 8328–8334.

[15] Chaudhari, A., Darvas, F., Bading, J., Moats, R., Conti, P., Smith, D., Cherry, S., Leahy, R. (2005). Hyperspectral and multispectral bioluminescence optical tomography for small animal imaging. *Physics in medicine and biology*, 50(23), 5421–5441.

[16] Gowen, A., O'Donnell, C., Cullen, P., Downey, G., Frias, J. (2007). Hyperspectral imaging an emerging process analytical tool for food quality and safety control. *Trends in Food Science & Technology*, 18(12), 590–598.

[17] Nikhil, P., Sankar, P. (1993). A review on image segmentation techniques. *Pattern recognition*, 26(9), 1277–1294.

[18] Yu Z. (2001). A review of recent evaluation methods for image segmentation. *Signal Processing and its Applications, Sixth International Symposium IEEE*, 1, 148–151.

[19] Baranda, A. (2015). *A hyperspectral imaging system using an acousto.optic tunable filter*. Master Thesis. Norwegian University of Science and Technology.

[20] Ali, M., Ramy, A., Lilian, D., Joseph, H., Mark, D. (2017). Hyperespectral image processing for detection and grading of skin erythema. *Proc. SPIE Medical Imaging 2017, Image Processing*.

[21] Peng, F., Xin, S., Quansen, S. (2017). Hyperespectral image segmentation via frequency-based similarity for mixed noise estimation. *Remote sensing*, 9(12), 1237.

[22] Konstantin, B., Vladimir, Y. (2017). Hyperespectral imaging acousto-optic system with spatial filtering for optical phase visualization. *J. Biomedical Optics*, 22(6), 066017.

[23] Dey, V., Zhang, Y., Zhong, M. (2010). A review on image segmentation techniques with remote sensing perspective. *ISPRS TC VII Symposium*.

[24] Devarshi, N., Pinal, S. (2014). A review on image segmentation clustering algorithms. *International Journal of Computer Science Information Technology*, 5(3), 3289–3293.

[25] Lorente, D., Aleixos, N., Gomez, J., Cubero, S., Navarrete, O., Blasco, J. (2012). Recent advances and applications of hyperspectral imaging for fruit and vegetable quality assessment. *Food and Bioprocess Technology*, 5(4), 1121–1142.

[26] Voloshinov, V., Gupta, N. (2004). Ultraviolet-visible imaging acousto-optic tunable filters in KDP. *Applied optics*, 43(19), 3901–3909.

[27] Tsai, C. (1990). *Guided-wave acousto-optics: interactions, devices, and applications*. Springer-Verlag, 23.

[28] Voloshinov, V., Tatyana, M., Vladimir, Y. (2002). Two-dimensional selection of optical spatial frequencies by acousto-optic methods. *Optical Engineering*, 41(6), 1273–1280.